Multi-scale (time and mass) dynamics of space objects
Proceedings IAU Symposium No. 364, 2022
A. Celletti, C. Galeş, C. Beaugé, A. Lemaitre, eds.
doi:10.1017/S174392132100140X

Dynamical constraints on the evolution of the inner asteroid belt and the sources of meteorites

Stanley F. Dermott[1], Dan Li[2] and Apostolos A. Christou[3]

[1]Department of Astronomy, University of Florida, Gainesville, FL 32611, US
email: sdermott@ufl.edu

[2]NSF's National Optical-Infrared Astronomy Research Laboratory, Tucson, AZ 85719, US
email: dan.li@noirlab.edu

[3]Armagh Observatory and Planetarium, College Hill, Armagh, BT61 9DG
email: Apostolos.Christou@armagh.ac.uk

Abstract. We have shown that in the inner belt the loss of asteroids from the ν_6 secular resonance and the 3:1 Jovian mean motion resonance accounts for the observation that the mean size of the asteroids increases with increasing orbital inclination. We have used that observation to constrain the Yarkovsky loss timescale and to show that the family asteroids are embedded in a background population of old ghost families. We argue that all the asteroids in the inner belt originated from a small number of asteroids and that the initial mass of the belt was similar to that of the present belt. We also show that the observed size frequency distribution of the Vesta asteroid family was determined by the action of Yarkovsky forces, and that the age of this family is comparable to the age of the solar system.

Keywords. asteroids

1. Introduction

Small fragments of many asteroids exist in our meteorite collections and while these fragments provide invaluable information on the origin and evolution of the remnants of the primitive building blocks that formed the rocky planets, some important dynamical questions remain unanswered. Ideally, we would like to link specific meteorites or meteorite classes to known asteroids. In one case at least, given the strong links between 4 Vesta and the HED meteorites, that goal has been achieved (McSween *et al.* 2013). We also have small samples of material from the near-Earth asteroid (NEA) Itokawa and soon we expect to have samples from the NEAs Ryugu and Bennu. However, these small NEAs are rubble-pile asteroids that originate from the collisional disruption of much larger main-belt asteroids. One aim of this paper is to discuss some of the dynamical constraints on the likely number of precursor asteroids in the inner main belt (IMB) that are the root sources of a large fraction of the NEAs and meteorites.

We assume that the asteroids accreted in two separate reservoirs of carbonaceous (CC) and non-carbonaceous (NC) material, interior and exterior to their current locations, and were then scattered by planetary perturbations into the present belt (Walsh *et al.* 2011; Kruijer *et al.* 2017). We also assume that after all planetary migration and the scattering that resulted from that migration ceased, further evolution of the dynamically excited belt was driven by: (1) the collisional and (2) the rotational destruction of asteroids (Dohnanyi 1969; Jacobson *et al.* 2014); (3) chaotic orbital evolution (Wisdom 1985;

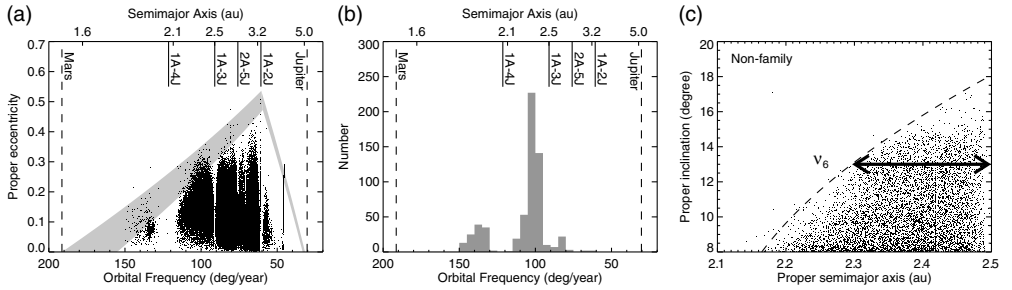

Figure 1. Panel (a): Scatter plot of the proper eccentricity e and the semimajor axis, a of the asteroids in the IMB with absolute magnitude $H < 15$. The shaded zone on the left is the Mars-crossing zone. Asteroids in that zone can, over time, cross the orbit of Mars. Panel (b): Histogram of the semimajor axes of the asteroids in the Mars-crossing zone. Panel (c): non-family asteroids in the IMB with $H < 16.5$ and high proper inclinations (Dermott *et al.* 2021).

Farinella *et al.* 1994; Morbidelli & Nesvorný 1999; Minton & Malhotra 2010); and (4) Yarkovsky-driven transport of small asteroids to the escape hatches located at orbital resonances (Migliorini *et al.* 1998; Farinella & Vokrouhlický 1999; Vokrouhlický & Farinella 2000). Insight into this dynamical evolution and estimates of the loss timescales are gained from an analysis of: (1) the observed variations with asteroid size of the mean orbital inclinations and eccentricities of the non-family asteroids; and (2) the size-frequency distributions of the small asteroids in the major families (Dermott *et al.* 2018; Dermott *et al.* 2021); (3) the cosmic-ray exposure ages of meteorites (Eugster *et al.* 2006); (4) the spin directions of near-Earth asteroids (Greenberg *et al.* 2020); and (5) the distribution of family asteroids in $a - 1/D$ space, where D is the asteroid diameter.

2. Asteroid size - orbital element correlations

The orbital eccentricities of main-belt asteroids are largely capped by the Mars-crossing zone (Fig. 1a) indicating that Mars has scattered some asteroids into the inner solar system. Most of the asteroids in the crossing-zone are in the inner main belt (IMB) (Fig. 1b), suggesting that the IMB is a major source of near-Earth asteroids (NEAs) and meteorites, a conclusion that is supported by the results of numerical investigations of the likely escape routes (Gladman *et al.* 1997; Granvik *et al.* 2017, 2018). Using the Hierarchical Clustering Method (HCM) developed by Zappala *et al.* (1990), Nesvorný (2015) has classified about half of the asteroids in the IMB with absolute magnitudes, $H < 16.5$ as family asteroids. But this fraction is an underestimate because some of the remaining asteroids are halo asteroids (Nesvorný *et al.* 2015), that is, they are also family asteroids, but because of the unavoidable limitations of the HCM it is not possible to classify these asteroids unambiguously. The remaining asteroids that are neither family nor halo asteroids are currently classified as non-family and an understanding of the evolution of the asteroid belt is not complete without an understanding of the nature and origin of these unclassified asteroids.

The family and halo asteroids are, by definition, tightly clustered in proper orbital element space. However, the family asteroids in that space are embedded in a background population of asteroids that could be members of old ghost families with dispersed orbital elements. To explore this background population, we need to find windows in orbital element space that are not obscured by the asteroids in the major families. Fortunately, one very large window exists in the IMB where all the asteroids in the major families and their halos have proper orbital inclinations, $I < 9$ *deg* (Dermott *et al.* 2018). In Fig. 1c, we see that the remaining non-family asteroids in the IMB with $I > 9$ *deg* are bound in $a - I$ space by the ν_6 secular resonance and the 3:1 Jovian mean motion resonance. These

https://doi.org/10.1017/S174392132100140X Published online by Cambridge University Press

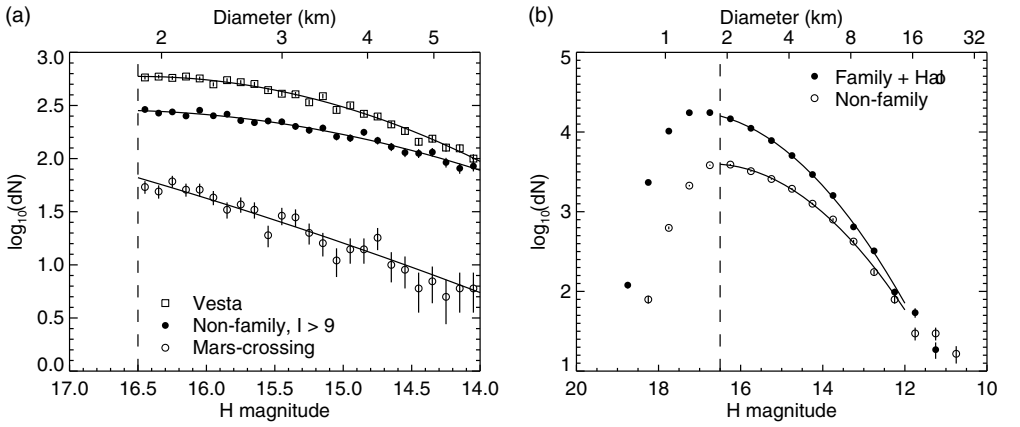

Figure 2. Panel (a): Quadratic polynomial fits to the SFDs of the asteroids in the Vesta family, for non-family asteroids with high inclinations ($I > 9$ *deg*), and for asteroids in the Mars-crossing zone. Panel (b): Comparison of the SFD of the non-family asteroids in the IMB with an estimate of the SFD of the family asteroids when combined with the asteroids in their halos.

resonances are two of the major escape hatches for asteroids in the IMB (Gladman *et al.* 1997; Granvik *et al.* 2017, 2018), but a third escape route is provided by a dense web of high-order Martian and Jovian resonances (Morbidelli & Nesvorný 1999; Milani *et al.* 2014) and we have argued that there is observational evidence that these high-order resonances also provide a significant loss mechanism (Dermott *et al.* 2021).

The size-frequency distribution (SFD) of the high inclination non-family asteroids shown in Fig. 2a shows a lack of small asteroids that is consistent with these asteroids being members of old ghost families that have lost small asteroids through collisional and rotational disruptions and the action of Yarkovsky forces. By assuming that the number density in $a - I$ space of the high-inclination, non-family asteroids shown in Fig. 1c applies to the IMB as a whole, we have shown that the fraction of asteroids in the IMB with $H < 16.5$ that are members of the major families or their halos is 76% and that the remaining 24% of the asteroids in the IMB are members of old ghost families (Dermott *et al.* 2021). If we further assume that the SFD of the high-inclination, non-family asteroids shown in Fig. 2a applies to all the non-family asteroids in the IMB and that the SFD of the halo asteroids (as a whole) is the same as that of the family members, then we can compare the SFD of the ghost family members with that of the family members and their halos. Accepting these simplifying assumptions, Fig. 2b shows that the smaller asteroids in the IMB with $H \sim 16$ are predominantly members of the major families. However, for asteroids with $H \lesssim 12$ and diameters, $D \gtrsim 16$ *km* this is not the case. This has several implications. Firstly, the probability of an asteroid that is currently classified as a family member being a family interloper increases with increasing asteroid size. Secondly, the fractions of the asteroids that are currently classified as S-type or C-type, etc., could change with asteroid size (see DeMeo & Carry 2014). Thirdly, our estimate of the number of asteroids that are the root sources of the NEAs and meteorites that originate from the IMB depends on the typical size of the asteroids whose disruption resulted in the injection of NEAs and meteorites into the inner solar system. Here, because the cosmic ray exposure ages of meteorites (Eugster *et al.* 2006) are much less than the ages of the asteroid families, we assume that the NEAs and meteorites do not originate directly from the initial disruptions of the root precursor asteroids, that is, from the events that formed the families, but from secondary disruptions of the family members. If the secondary asteroids were totally disrupted and typically had diameters

https://doi.org/10.1017/S174392132100140X Published online by Cambridge University Press

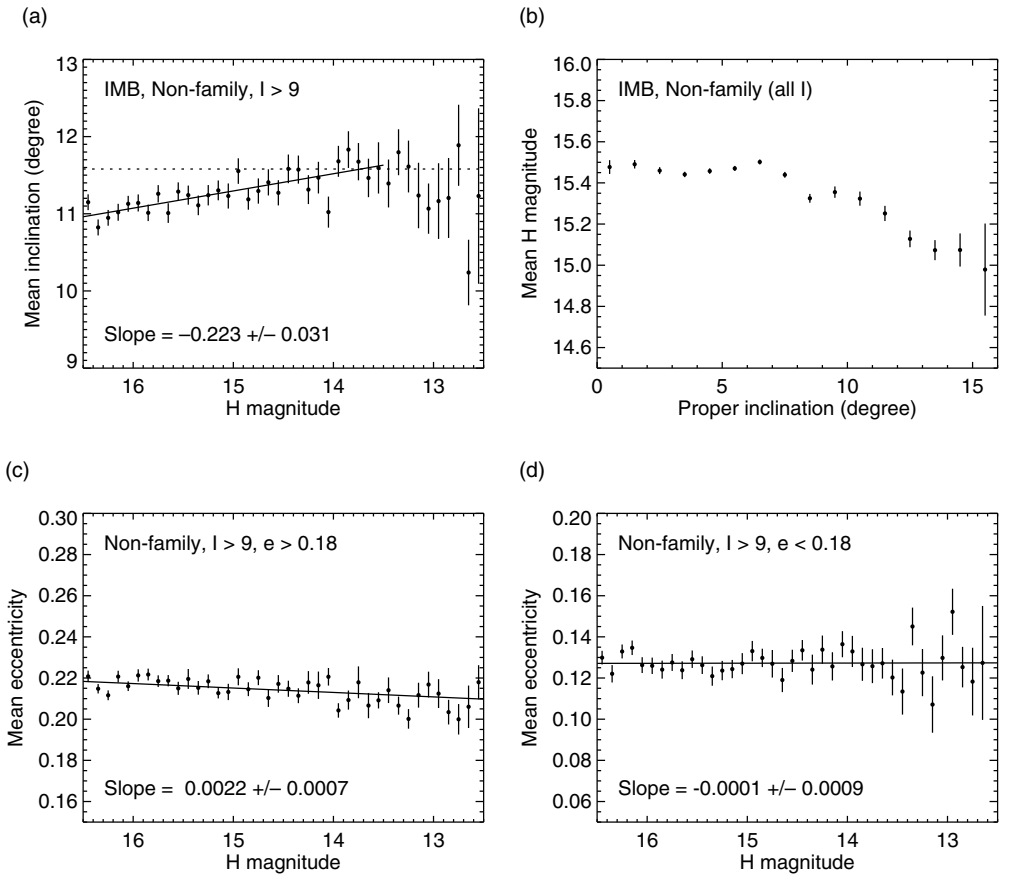

Figure 3. Panel (a): Variation with absolute magnitude, H of the mean proper inclination of the high inclination ($I > 9$ *deg*), non-family asteroids. The data is shown binned in H, but the slope has been determined from the individual points in the range $16.5 > H > 13.5$. Panel (b): Variation with proper inclination, I of the mean absolute magnitude, H of the all the non-family asteroids in the IMB. Panel (c): Variation with absolute magnitude, H of the mean proper eccentricity of the high inclination ($I > 9$ *deg*), non-family asteroids with $e > 0.18$. Panel (d) A similar plot to Panel (c) for those asteroids with $e < 0.18$ (Dermott *et al.* 2021).

$\sim 1\ km$, as suggested by Jenniskens (2020), then these asteroids were most likely members of the 5 or 6 major families currently dominating the IMB in that size range (Fig. 2b). This estimate of the number of precursors is small and could be reduced even further by considering the proximity of the major families to the most likely escape hatches. However, if the meteorite sources were larger, then we must also consider the asteroids in the ghost families as possible precursors, and this increases our estimated number of root precursors to $\lesssim 20$ (Dermott *et al.* 2021).

Asteroids are lost from the IMB through at least four mechanisms: collisional and rotational destruction, chaotic orbital evolution, and Yarkovsky-driven transport of small asteroids to the resonant escape hatches. The timescales of these loss mechanisms are uncertain and there is a need for observational constraints. Of particular interest are the observed correlations between the mean asteroid sizes and their proper orbital elements. In Fig. 3a, we see that the mean proper inclination of the high-inclination ($I > 9$ *deg*), non-family asteroids in the IMB increases with increasing asteroid size. In contrast, in

https://doi.org/10.1017/S174392132100140X Published online by Cambridge University Press

Fig. 3c we see that the mean proper eccentricity of the high-eccentricity asteroids (that also have high inclination), increases with decreasing asteroid size. The size-inclination correlation can be accounted for by the action of Yarkovsky forces driving small asteroids to the two bounding resonances (Dermott *et al.* 2021). The length of the escape route (Fig. 1c) decreases with increasing inclination and this leads, inevitably, to a correlation between the sizes and inclinations of the remaining asteroids. The distribution of the asteroids in $a - I$ space shown in Fig. 1c appears to be approximately uniform. If we assume that the initial distribution was also uniform, that is, not dependent on a or I, then the observed size-inclination correlation is determined by the Yarkovsky timescale alone and this timescale can be determined without knowing the initial SFD. We write

$$\frac{1}{a}\frac{da}{dt} = \pm\left(\frac{1}{T_Y}\right)\left(\frac{1\,km}{D}\right)^{\alpha}, \tag{1}$$

where T_Y is the Yarkovsky timescale and the coefficient α is determined by the size dependence of the Yarkovsky force. The other loss mechanisms that do not depend on the orbital inclination include the net effect of catastrophic destruction and creation, and rotational disruption. These loss mechanisms are size dependent and should be modeled separately, but we are able to show that, in the size range that we model, Yarkovsky loss is the dominant loss mechanism and therefore it is expedient to reduce the number of variables in our models by writing

$$\frac{1}{N(D)}\frac{dN(D)}{dt} = -\left(\frac{1}{T_L}\right)\left(\frac{1\,km}{D}\right)^{\beta}, \tag{2}$$

where T_L is the timescale of the combined inclination-independent loss mechanisms and $N(D)$ is the number of asteroids of diameter D.

Some of our model results, obtained using both loss mechanisms, are shown in Fig. 4. By adjusting the values of the five parameters b, α, T_Y, β, T_L, we can account for both the observed size-inclination correlation (Figs. 4c and 4f) and the observed SFD (Fig. 4b). These results show that for asteroids with absolute magnitudes in the range $13.5 < H < 16.5$, Yarkovsky transport of asteroids to the resonant escape hatches is the dominant loss mechanism (Fig. 4a). This conclusion is supported by the model results shown in Figs. 4d and 4e in which we use the Yarkovsky loss mechanism alone. For asteroids with $H < 16.5$ the inclination-independent asteroid loss mechanism has only a small effect on the fit for the SFD, and no effect on the observed asteroid size-inclination correlation. There is a large difference to the SFD fit for those asteroids with $H > 16.5$, but, at present, these very small asteroids are observationally incomplete. When the IMB completeness level has been extended from $H = 16.5$ to, say, $H = 18$, we will be able to constrain the loss timescales for the collisional and rotational disruption of the asteroids.

Using both loss mechanisms, we calculate that if these mechanisms have operated without change over the age of the solar system, then the Yarkovsky loss timescale, T_Y needed to account for the size-inclination correlation is 13.4 Gyr. This timescale is unacceptably longer than the result, $T_Y \approx 4$ Gyr for asteroids with $a = 2.4$ au derived from the value that Greenberg *et al.* (2020) obtained from an analysis of the orbital evolution of 247 small NEAs. If the Yarkovsky timescale was as short as 4 Gyr, then many more asteroids would have been lost from the IMB and the size-inclination correlation would have been much stronger. We have argued that the most likely explanation for this large discrepancy is that the asteroids in the IMB are not as old the solar system but are collision products and members of old ghost families. However, this explanation for the observed size-inclination correlation needs to be explored further. Previously, we

https://doi.org/10.1017/S174392132100140X Published online by Cambridge University Press

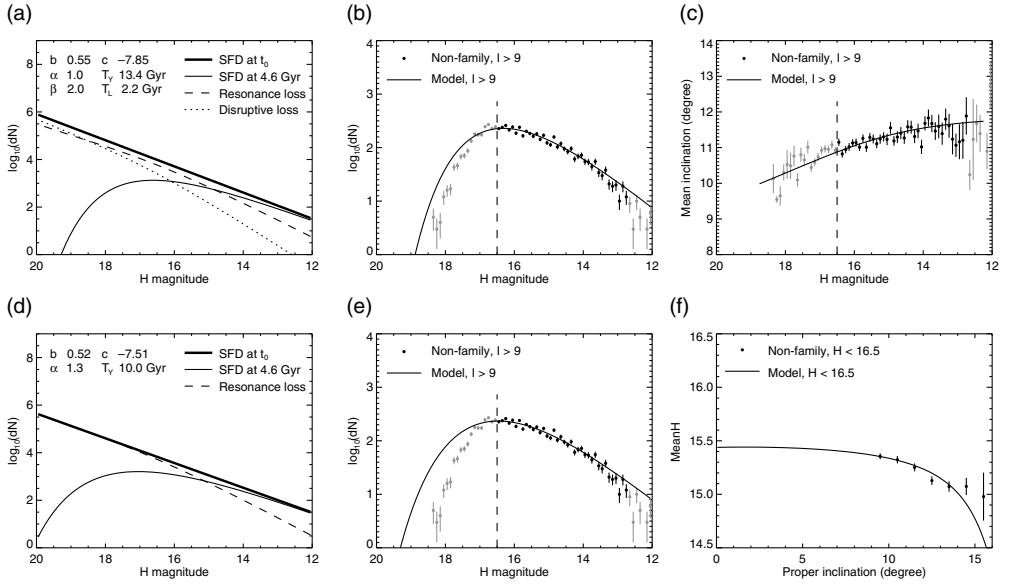

Figure 4. Models for the depletion of all the high-inclination, non-family asteroids in the IMB due to a Yarkovsky force that changes the semimajor axes on a timescale $T_{\rm Y}$, and all other loss mechanisms that do not depend on the proper inclination, I and result in the loss of asteroids on a timescale $T_{\rm L}$. α and β describe the dependence of these two timescales on the asteroid diameter.

argued that the asteroid size-orbital element correlations of the non-family asteroids in the IMB are evidence for the existence of ghost families (Dermott *et al.* 2018), because if we had, say, two families and the members in one family had a common inclination that was different from the common inclination of the members in the second family, and if these two families had different SFDs, then merging these two families could result in a ghost family with correlated inclinations and sizes. The difference between these two ideas is that the Yarkovsky loss model results, inevitably, in a size-inclination correlation of predictable sign and magnitude, whereas with the second idea a correlation of unpredictable sign and magnitude is only a possibility. If the number of merged families increases, then the possibility of a significant correlation due to the second mechanism alone decreases. However, what these two ideas have in common is that they both argue for the existence of ghost families, and we now need to examine other evidence for the existence of these families.

Figure 5 is a scatter plot of the high-inclination, IMB asteroids in $e-I$ space. Using the WISE albedos (Masiero *et al.* 2014), these asteroids have been separated into CC and NC groups. About 12% of the asteroids are members of small families (Figs. 5a and 5b). The remaining 88% (Figs. 5c and 5d) are non-family asteroids. Inspection of this figure shows that some of the CC non-family asteroids could be halo asteroids originating from the Klio and Chaldaea families, but some other apparent clumps could be large ghost families. The SFDs of the non-family CC and NC asteroids are shown in Fig. 6. These SFDs are significantly different which could indicate families of different ages. However, this is not a reliable conclusion because only about half of the IMB asteroids with $H < 16.5$ have WISE albedos and therefore the data set is incomplete and not bias free. A more reliable indication of the existence of ghost families is the observation that the CC and NC asteroids have markedly different mean eccentricities and inclinations (Dermott *et al.* 2021).

https://doi.org/10.1017/S174392132100140X Published online by Cambridge University Press

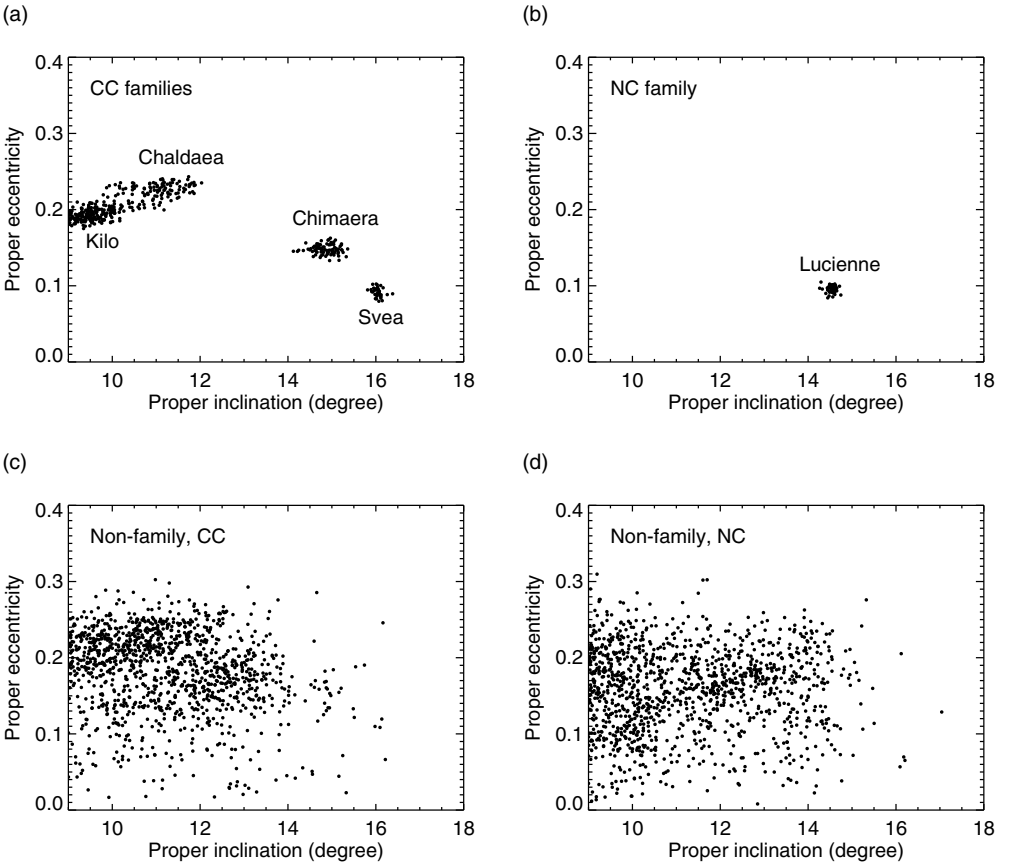

Figure 5. The asteroids in the IMB with high inclinations have been divided into two groups of CC and NC asteroids according to their WISE albedos, A (Masiero *et al.* 2014). CC have $A < 0.13$ and NC have $A > 0.13$. The panels show e and I scatter plots of all the asteroids with $H > 16.5$ divided into CC and NC family and non-family groups.

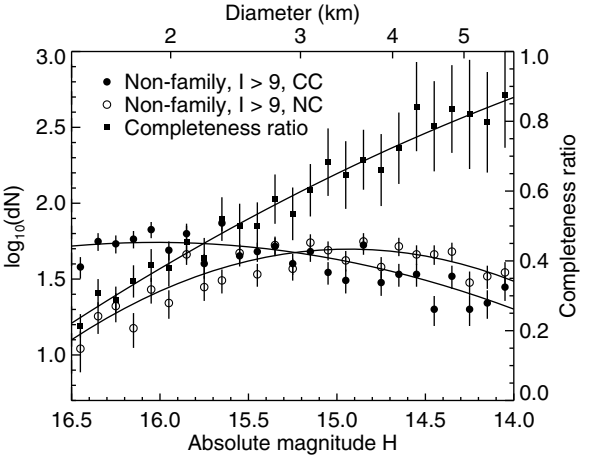

Figure 6. Comparison of the SFDs of the CC and NC non-family asteroids in the IMB with $I > 9$ *deg* and $H < 16.5$. The completeness ratio is the fraction of the asteroids with WISE albedos.

https://doi.org/10.1017/S174392132100140X Published online by Cambridge University Press

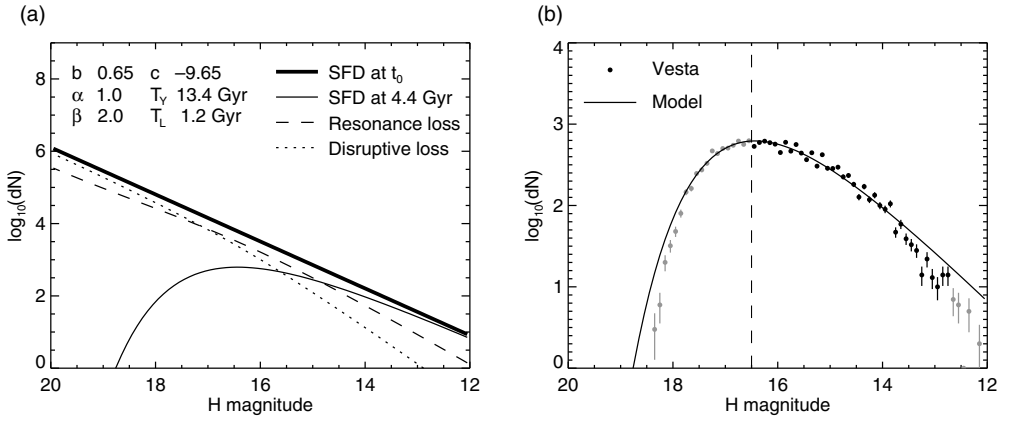

Figure 7. Panel (a): model for the loss of the Vesta family asteroids due to a Yarkovsky force that changes the semimajor axis on a timescale $T_{\rm Y}$, and to all other loss mechanisms that do not depend on the proper inclination that change the semimajor axis on a timescale $T_{\rm L}$. α and β describe the dependence of these timescales on the asteroid diameter, D. The constant b is the slope of the initial SFD and c is a normalizing constant that determines the total number of asteroids in the distribution.

3. The age of the Vesta asteroid family

The asteroid families were created either by collisional disruptions or by cratering events on large asteroids. In either case, if we assume that the SFD of the small asteroids in a family was initially linear on a log-log scale, as observed for the young Massalia family, then our models allow us to determine the age of the family and the initial slope, b of the incremental SFD that we assume had the form

$$\log dN = bH + c, \tag{3}$$

where dN is the number of asteroids in a box of width dH and c is a constant for asteroids with the same albedo. Because the asteroids in a family have, by definition, approximately the same inclination, and because the slope, b of the initial SFD is an unknown parameter, we only have one observational constraint on our model and that is the current SFD. Model results for the SFD of the Vesta family (Fig. 2) are particularly interesting. This family was probably formed by the impact that created the giant $\sim$500 km diameter and $\sim$20 km deep Rheasilvia basin that overlies and partially obscures the smaller ($\sim$400 km diameter) and older Veneneia crater (Marchi *et al.* 2012). Our model results are shown in Fig. 7. We allow that the age of the family, $t_{\rm Vesta}$, the initial slope of the SFD, b, and the timescale of the inclination-independent loss mechanism, $T_{\rm L}$, are free parameters, but set $\alpha = 1$, $\beta = 2$ and $T_{\rm Y}$ to the best-fitting value derived from the model for the high-inclination ($I > 9$ deg), non-family asteroids shown in Fig. 4. The results are only partly satisfactory because our best-fit solution has $b = 0.65$ which is slightly greater than the upper limit, $b = 0.6$, determined by the condition that the total mass in the distribution cannot be infinite (Durda & Dermott 1997). Noting that our models only derive ratios of timescales, our best model (Fig. 7) gives

$$t_{\rm Vesta}/T_{\rm Y} = 0.33 \pm 0.015. \tag{4}$$

If we assume that the mean density of the Vestoids is 2850 $kg\ m^{-3}$ (Jenniskens *et al.* 2021) - a value that is larger than the density of 2000 $kg\ m^{-3}$ assumed in our earlier paper (Dermott *et al.* 2021), then using the Greenberg *et al.* (2020) NEA observations and their estimate that the thermal efficiency, $\xi = 0.12$, we estimate that $T_{\rm Y} = 6$ Gyr and $t_{\rm Vesta} = 2.0 \pm 0.1$ Gyr. This age is greater than the age $\sim$1.3 Gyr obtained from Vesta

https://doi.org/10.1017/S174392132100140X Published online by Cambridge University Press

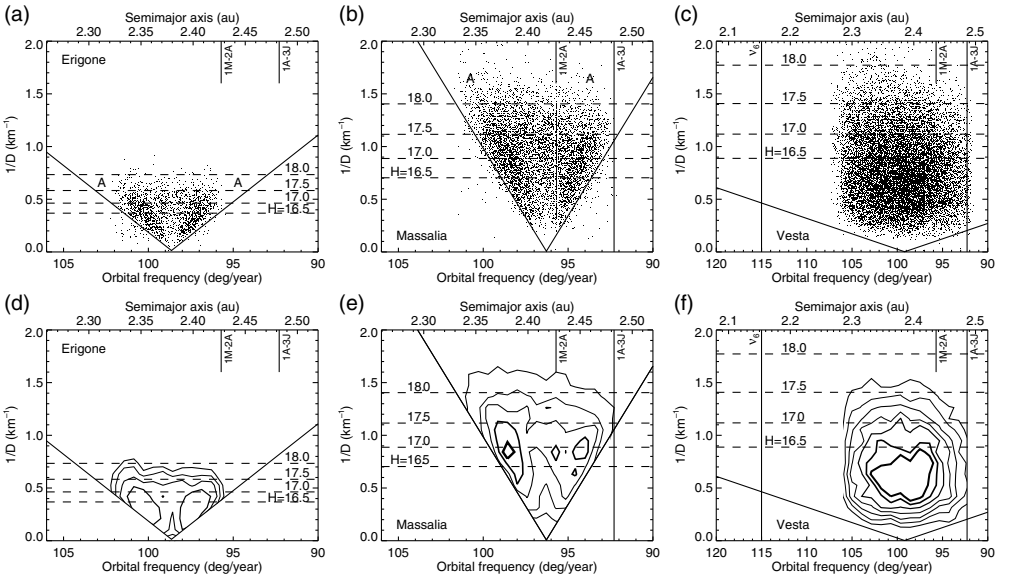

Figure 8. V-shaped distributions in $1/D - a$ space of the asteroids in the Erigone, Massalia and Vesta families with no limit on H. Diameters, D have been calculated assuming albedos of 0.06, 0.22 and 0.35 for, respectively, Erigone, Massalia and Vesta. The V-shaped lines for Massalia correspond to the fit determined by Milani *et al.* (2014). The lower panels are the corresponding number density plots with linear spacing of the contour plots.

surface crater counts (Marchi *et al.* 2012). However, the difference between these two age estimates could be even larger. Using the NEA orbital evolution timescale implies that the orbital evolution rates are constant, and we consider that to be unlikely. The NEA observations do not allow for asteroid disruptions or for changes in the asteroid spin directions and therefore the NEA observations are not applicable to the small asteroids in a family that is old. Thus, our estimate of the age of the Vesta family is likely to be a significant underestimate. We note that for both the high-inclination, non-family asteroids and the Vesta family, $t_{\rm evol}/T_{\rm Y} = 1/3$ (where $t_{\rm evol}$ is the average time of orbital evolution), consistent with our argument that both groups of asteroids have had similar evolutionary histories and therefore that both have ages comparable with the age of the solar system.

We support this conclusion by considering the dynamical evolution of small asteroids due to mechanisms other than Yarkovsky driven orbital evolution. The observations and models shown in Figs. 2, 4 and 7 reveal that the incremental SFDs of all the family and non-family asteroids are close to peaks at $H = 16.5$. For asteroids with $H < 16.5$, Yarkovsky loss is the dominant loss mechanism. The asteroids with $H > 16.5$ may not be observationally complete, but our models suggest that the number of small asteroids drops off sharply with increasing H. Small asteroids may be created by the disruption of larger asteroids, but this must be at a rate less than the loss rate. The distributions in $a - 1/D$ space of the asteroids in the Erigone, Massalia and Vesta families are shown in Fig. 8. The three sets of V-shaped lines correspond to ages of 1.6 10^8 Gyr (Erigone), 1.6 10^8 Gyr (Massalia) and 1.3 10^9 Gyr (Vesta). These ages were calculated using Yarkovsky timescales calculated from the NEA observations (Greenberg *et al.* 2020) for asteroids with $a = 2.4$ au, assuming asteroid densities of 1570 kg m^{-3} (Erigone), 3000 kg m^{-3} (Massalia) and 2850 kg m^{-3} (Vesta, Jenniskens *et al.* (2021)). These three families were formed by cratering events (Spoto *et al.* 2015). However, their distributions in $a - 1/D$ space show significant differences. In Fig. 8a, we see that in the young Erigone family,

https://doi.org/10.1017/S174392132100140X Published online by Cambridge University Press

the distribution of the larger asteroids with inverse diameters, $1/D \lesssim, 0.5$ has two well-separated lobes and a central depletion, consistent with orbital evolution at a constant rate driven by Yarkovsky forces without significant asteroid disruptions or changes in spin direction. However, for the smaller asteroids with $1/D \gtrsim 0.5$, we see an absence of a central depletion suggesting that these very small asteroids have experienced significant changes in their spin directions and/or collisional disruptions with the result that their orbital evolution may have been more of a random walk (Marzari *et al.* 2020; Dermott *et al.* 2021; Dell'Oro *et al.* 2021). We also see an absence of very small asteroids with high $1/D$ at the two extremes of the V-shaped distribution (marked in Fig. 8a with an A) suggesting, perhaps, that the very small asteroids in the family experienced disruptions preventing them from evolving to those extreme locations. However, this conclusion is not secure because any collisional disruption of the larger asteroids in the family would have produced an enhancement of the number density of small asteroids with high $1/D$ in the central region of the V-shaped distribution. In Fig. 8b, we observe that the young Massalia family has a distribution like that of the Erigone family, although for this family the loss of the central depletion occurs for those asteroids with $1/D \gtrsim 1.2$. Significantly, in Fig. 8c, we see that the distribution for the Vesta family is markedly different from both young families. For Vesta, the central depletion is absent at all diameters suggesting that most of the small asteroids in the Vesta family have experienced collisional evolution and/or significant changes in their spin directions, supporting our argument, based on the observed SFD, that the Vesta family could have an age comparable with the age of the solar system.

The plots in Fig. 8 for the Erigone and Massalia families contain information on the dynamical evolution of the families in addition to their ages. This may allow us to determine the timescale, T_{L} of the combined inclination-independent loss mechanisms separately from our estimate of the Yarkovsky loss timescale, but this information may only be useful when the observational completeness limit has been extended to, say, $H \sim 18$. The Erigone and Massalia families have approximately the same mean semimajor axis. Therefore, the degree of completeness of each family for a given value of H should be closely similar, although we note that the Erigone family has a mean eccentricity, $e = 0.191$ which is slightly greater than the mean value, $e = 0.142$, of the Massalia family, making the Erigone family asteroids slightly easier to discover. Current estimates of the observational completeness limit at $a = 2.4$ au are $H = 16.5$ (Dermott *et al.* 2018) and $H = 17.6$ (Hendler & Malhotra 2020). For families with ages greater than the timescale for the loss of asteroids of diameter D_{L} due to mechanisms other than Yarkovsky loss, we should observe a drop off in the number density of asteroids in $a - 1/D$ space of those asteroids with diameters $D < D_{\mathrm{L}}$, consistent with the observed shape of the SFD. For Erigone, which is a C-type asteroid with an albedo, A 0.06, there is a marked drop off in the number of asteroids with $H \gtrsim 17.0$, whereas for Massalia, which is an S-type asteroid with A 0.22, the drop off occurs for those asteroids with $H \gtrsim 18.0$. These values of H correspond to diameters $\sim$2.2 km for Erigone and $\sim$0.7 km for Massalia. While recognizing that for $H \gtrsim 17.0$ the distributions may be observationally incomplete, it is worth discussing the information that will be available when the completeness limit is extended to $H \sim 18.0$.

The Erigone and Massalia families both appear to have an age of $\sim 1.6\ 10^8$ Myr, although this estimate assumes that the Yarkovsky timescale can be deduced from the NEA observations with allowance for the differences in the mean densities, but with no allowance for possible differences in their thermal efficiencies, even though these asteroids are of different types. We also note that the mean value of the thermal efficiencies of the NEAs is an average value that does not distinguish between NEAs of different types. The number of asteroids with $H < 16.5$ in the Massalia family is 1450, whereas the

https://doi.org/10.1017/S174392132100140X Published online by Cambridge University Press

corresponding number in the Erigone family is 777. This difference of a factor of 2 is not enough to account for the observation that the number of asteroids in the Massalia family with $H > 17.5$ is 1859, whereas for the Erigone family the number is 166. If this large difference is not due solely to observational selection, then it suggests that C-type asteroids of a given diameter are easier to disrupt than S-type asteroids. We note that Morbidelli *et al.* (1997) consider that there is observational evidence that C-type NEAs may be easier to disrupt than S-type NEAs.

Small asteroids are lost through Yarkovsky forces, rotational disruption, and catastrophic collisions. With respect to the latter mechanism, we note that because of their near identical locations in the IMB, that only differ because of the small differences in their mean eccentricities and inclinations, the two families are impacted by a common population of asteroids. If the asteroids are rubble-piles, then the critical mass, m of the asteroid bullet needed to overcome the gravitational forces binding an asteroid of mass M is given by

$$f\frac{1}{2}mV^2 = \frac{12GM^2}{5D}, \tag{5}$$

where V is the impact velocity and f is the fraction of the kinetic energy available to disrupt the larger asteroid. This implies that the critical diameter for asteroids of a given age varies as

$$D_{\rm L} \propto \left(\frac{f}{\rho^2}\right)^{1/5}, \tag{6}$$

where ρ is the bulk density. Thus, $D_{\rm L}$ increases with decreasing density and increasing f, but to account for C-type and S-type asteroids in families of approximately the same age having values of $D_{\rm L}$ that differ by a factor as large as 2, we need f/ρ^2 to differ by a factor of 2^5. If we ignore the differences in the values $D_{\rm L}$ and assume that for both families the number drop-off occurs for $D_{\rm L} \sim 1\ km$, then the collisional lifetime of these 1 km asteroids is $\sim$1.6 10^8 yr, the estimated age of the families. Jacobson *et al.* (2014) argue that collisional disruption is not the dominant loss mechanism because YORP forces increase the spin rates and drive asteroids to destruction on a timescale given by

$$T_{\rm YORP} = 10\ Myr \left(\frac{D}{1\ km}\right)^2. \tag{7}$$

This is a factor $\sim$10 less than our very rough estimate of the non-Yarkovsky loss timescale and a timescale as small as 10^7 yr appears to conflict with the observations. However, these conclusions are not firm, partly because of possible observational incompleteness, but also because it is not known how the Yarkovsky loss timescale, that determines the age of the families, varies with asteroid type.

4. Martian mean motion resonances

Greenberg *et al.* (2020) determined from observations of the orbital evolution of 247 NEAs that the ratio of the retrograde to prograde spins of these objects is as high as $2.7^{+0.3}_{-0.7}$ and argued, following Nugent *et al.* (2012) and Fanocchia *et al.* (2013), that this ratio places bounds on the fraction of the NEAs that are scattered into the inner solar system through the ν_6 secular resonance. If this resonance and the Jovian 3:1 mean motion resonance were the only escape hatches from the IMB, and if asteroids with both retrograde and prograde spins escape through the 3:1 resonance, but only asteroids with retrograde spins and shrinking semimajor axes escape through the ν_6 resonance, then their conclusion that the ν_6 resonance is the dominant escape route is valid. However, in the IMB we observe that the mean proper eccentricity of the non-family asteroids increases with decreasing asteroid size (Fig. 3c). In addition, the proper

https://doi.org/10.1017/S174392132100140X Published online by Cambridge University Press

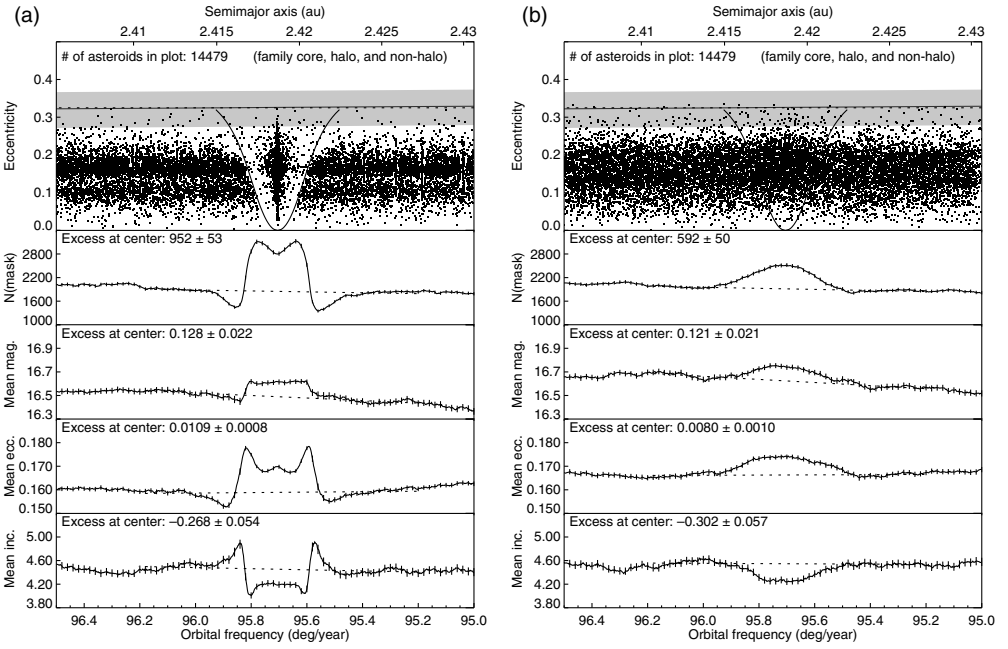

Figure 9. Panel (a): Scatter plot of the proper eccentricities and semimajor axes of the asteroids near the Martian 1:2 mean motion resonance (no limit on H). The mask shown in the top panel is based on the maximum libration width of the strongest term in the disturbing function of the resonance. By sliding this mask through the asteroid population, we compare the mean values of the number density, the mean absolute magnitude, the mean proper eccentricity, and the mean proper inclination of those asteroids trapped in the resonance with those of their near neighbors. Panel (b): A similar plot based on sliding the same mask through the osculating orbital elements.

inclinations of the asteroids in the Mars-crossing zone have distributions in $a - I$ space like those of the asteroids in the major families and, for asteroids with the observed distribution of semimajor axes, the inclinations are mostly too low for the asteroids to have entered the Mars-crossing zone through the ν_6 resonance. Following the work of Morbidelli & Nesvorný (1999), we have argued that these two observations suggest that the escape of asteroids through a dense web of high-order mean motion resonances may be a significant loss mechanism. Yarkovsky forces will feed the asteroids into these high-order resonances, and it may be that the asteroids with retrograde spins experience increases in their eccentricities and escape at a greater rate than those with prograde spins. However, obtaining numerical results to support this suggestion, that consider the passage of asteroids through many high-order resonances, and include both point-mass gravitational forces, that do not depend on the sense of asteroid rotation, and size-dependent Yarkovsky forces, is a task that has not yet been undertaken.

Here, we discuss the simpler problem of the dynamics of the Martian 1:2 mean motion resonance. Gallardo (2007); Gallardo *et al.* (2011) was the first to show that, in contrast to the prominent Kirkwood gaps in the main belt, this Martian resonance has a large excess of asteroids and the asteroids in the resonance have different mean sizes, mean eccentricities, and mean inclinations from those of their non-resonant near-neighbors. These observed differences can be quantified precisely, and with further work they could shed light on the role of the Martian mean motion resonances in the dynamical evolution of the IMB. The top panel in Fig. 9a is a scatter plot of the proper eccentricities and

https://doi.org/10.1017/S174392132100140X Published online by Cambridge University Press

semimajor axes of the asteroids close to the Martian 1:2 mean motion resonance (no limit on H). Note that this plot contains 14,479 asteroids and has a total width of only $\sim$0.02 *au*. The mask shown in this panel is based on the maximum libration width of the strongest term in the disturbing function of the resonance, calculated using the full disturbing function with the simplifying assumption that the orbits are coplanar.

The approximate width, Δa of the 1:2 first-order resonance that defines the libration mask is given by

$$\frac{\Delta a}{a} = 0.00341\sqrt{e}. \tag{8}$$

By sliding the libration mask through the asteroid population, we can compare the mean values of the number density, the mean absolute magnitude, the mean proper eccentricity, and the mean proper inclination of the asteroids trapped in the resonance, defined here as lying within the libration mask, with those of their near-neighbors. We observe that the number of asteroids residing in the resonance is clearly excessive, and that those asteroids have higher mean proper eccentricities, are smaller, and have lower mean proper inclinations, than their near-neighbors. The plots in Fig. 9a are based on the synthetic proper orbital elements obtained by Knežević & Milani (2000) by numerically integrating the orbits of the planets and asteroids over millions of years and extracting the forced and proper elements by filtering. Their integrations do not include Yarkovsky forces, even though, for very small asteroids, the effects of these forces may not be negligible. One could question the use of proper, or long-term average, orbital elements when any analysis of the dynamics of resonance involves the osculating elements. For those reasons, in Fig. 9b we have included plots based on the osculating elements. The changes that we observe with the osculating elements are like those obtained with the proper elements shown in Fig. 9a, although there are differences in the magnitudes of those changes. In future work, involving the numerical integration of the orbits of the asteroids as they evolve through the resonance under the action of Yarkovsky forces, the observations for the osculating orbits should prove to be the most useful because they can be compared directly with the results of the numerical integrations without the use of any filters.

The dynamics of first-order resonance involving satellites with small eccentricities and well-separated libration frequencies and widths, such that only one resonant argument needs to be retained in the analysis, has had many successful applications. But the Martian 1:2 resonance for asteroids with moderate eccentricities is a multiplet consisting of many significant overlapping resonances and those methods cannot be universally applied. For example, simple first-order theory predicts that capture into resonance can occur only if asteroids are evolving on converging orbits, that is, towards the resonance and towards Mars (Murray & Dermott 1999), and that the probability of capture into resonance decreases markedly with increasing eccentricity. But Gallardo *et al.* (2011) has shown through numerical integrations that capture into resonance can occur for asteroids with large eccentricities, evolving on both converging and diverging orbits. We observe that the libration mask, based on a single resonant argument, does give a good account of the distribution of the proper eccentricities for $e \leq 0.2$ (Fig. 9a), but breaks down for higher eccentricities. This could be partly because gravitational interactions between the Martian 1:2 resonance and the 3:1 Jovian resonance result in two series of 3-body resonances with asteroid frequencies, n_A given by

$$n_{\rm A} - 3n_{\rm J} = k(n_{\rm M} - 2n_{\rm A}), \tag{9}$$

where the integer $k = \pm(1, 2, 3, ...)$ and the mean motions of the asteroid, Mars and Jupiter are denoted, respectively, by $n_{\rm A}$, $n_{\rm M}$ and $n_{\rm J}$. These 3-body resonances have mean motions, $n_{\rm A}$ either greater or less than $n_{\rm M}/2$, depending on the sign of k. As $|k|$

https://doi.org/10.1017/S174392132100140X Published online by Cambridge University Press

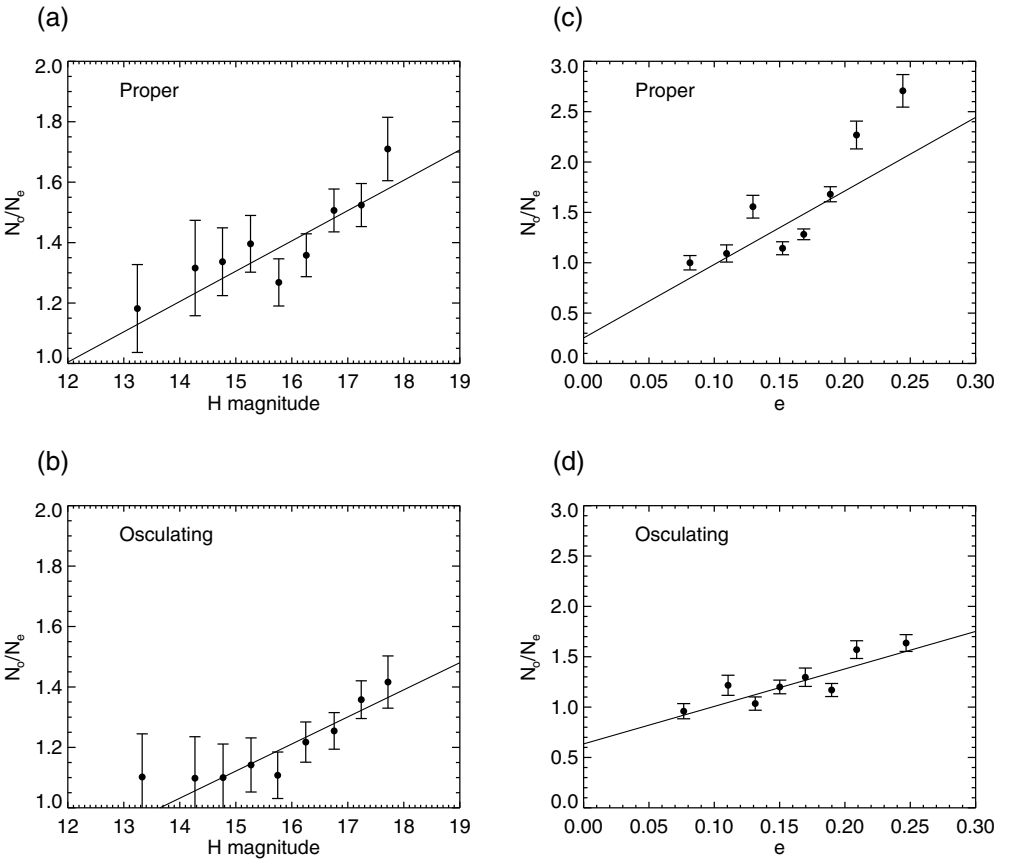

Figure 10. Plots of the variation of the excess number of asteroids trapped in the 1:2 Martian resonance with, on the left, absolute magnitude and, on the right, orbital eccentricity. The upper and lower plots show, respectively, the proper and the osculating elements.

increases, the separation of neighboring resonances, $\Delta n_{\rm A}$ decreases as

$$\Delta n_{\rm A} = (n_{\rm M}/2 - n_{\rm A})/k \tag{10}$$

and both series converge on the Martian 1:2 resonance. These 3-body resonances account for the columns of asteroids with $e \sim 0.2$ shown in Fig. 9a. As $|k|$ increases, the 3-body multiplets become close enough to overlap, resulting in a highly chaotic zone that extends well beyond the bounds of the libration mask. This could account for the observed lack of asteroids with $e \gtrsim 0.2$ immediately outside of those bounds (Fig. 9a).

The number of asteroids shown in Fig. 9 is 14,479 (no limit on H). This number is so high that we can usefully divide the population into several subgroups. In Fig. 10 we show, using both the proper and the osculating orbital elements, how the number excess in the libration mask varies with absolute magnitude and eccentricity. If we consider the passage of the asteroids through the resonance as a flow problem, then the ratio of the observed to the expected number of asteroids in the mask, $N_{\rm o}/N_{\rm e}$, is determined by the ratio of the average time, $\Delta t_{\rm mask}$ that the asteroids reside within the mask to the time needed by the asteroids to traverse the width of the mask in the absence of the resonance, as determined by the Yarkovsky timescale. This argument does not require the asteroids to have a common direction of flow. From eqns. (1) and (8), we obtain

$$\Delta t_{\rm mask} = 0.00341 (N_{\rm o}/N_{\rm e}) T_{\rm y} (D/1\,km) \sqrt{e}. \tag{11}$$

https://doi.org/10.1017/S174392132100140X Published online by Cambridge University Press

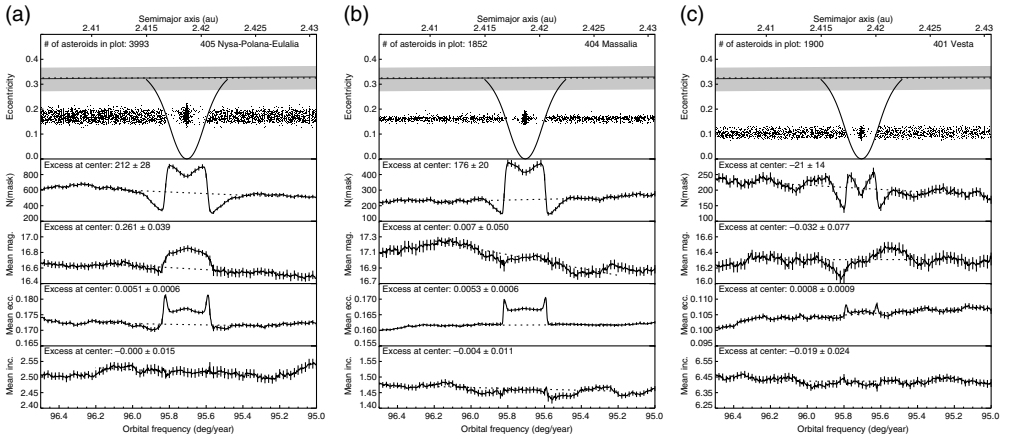

Figure 11. These plots are similar to those shown in Figure 9 and use the proper elements of the asteroids in (a) the Nysa-Polana-Eulalia family complex, (b) the Massalia family, and (c) the Vesta family (no limit on H).

The mean osculating e of the asteroids in Fig. 10b is 0.166. Assuming an average albedo, A of 0.13, $H = 16$ corresponds to a diameter, D of 2 km. The observed number excess for $H = 16$ shown in Fig. 10b is 1.2. Assuming that $T_{\rm y} = 4\ Gyr$, we calculate that $\Delta t_{\rm mask} = 13\ Myr$. This is probably less than both the collisional lifetime and the timescale for changes in the spin directions, suggesting that the changes due to the resonance that we observe in Fig. 10 are caused solely by the actions of gravitational forces and Yarkovsky forces. Thus, it should be possible, through numerical experiments, to determine the magnitudes of the Yarkovsky forces from the observations. However, we need to discuss some problems with this suggestion.

In Fig. 9, we observe that the resonance has an excess number of asteroids and that the asteroids are, on average, smaller than their neighbors. This suggests that Yarkovsky forces transport small asteroids to the resonance, and this is supported by the observations shown in Fig. 10 that the various changes are size dependent. We also observe an increase in the mean eccentricity. Point-mass gravitational forces acting alone on asteroids trapped in the Martian 1:2 resonance increase the dispersions of the eccentricities and inclinations, but they do not change their mean values (Christou *et al.* 2020). However, if the spin directions of the asteroids in the resonance are not random, then Yarkovsky forces will act to change the mean eccentricities, but the changes in the mean inclinations will be very much less than any changes in the mean eccentricities, and this conflicts with the observations. However, the large changes in the mean inclination observed in Fig. 9 can be explained by the existence of discrete families in the IMB. Consider two families of comparable size that have distinctly different mean inclinations and eccentricities. In Fig. 10 we observe that the number excess varies with eccentricity. Therefore, if the families have different mean eccentricities, then we might expect these families to have different number excesses and it follows that the mean inclination of the combined families outside of the resonance will differ from that of the asteroids in the resonance, even though the change in the mean inclination of each family is zero.

We support this argument by analyzing the distributions of the asteroids in the separate families. When we separate the asteroids shown in Fig. 9 into families, we observe that in each case the change in the mean inclination is zero. Fig. 11a is for the Nysa-Polana-Eulalia complex, which consists of at least two families, but these families have a common mean eccentricity and this may explain why the inclination change is zero. Fig. 11b is for the Massalia family, a young family that appears to be devoid of any secondary families.

https://doi.org/10.1017/S174392132100140X Published online by Cambridge University Press

For this family, we observe a large number excess and an increase in the mean eccentricity, but zero change in the mean inclination. However, for this family we also observe zero change in the mean size of the asteroids in the libration mask as compared with their near-neighbors, undermining the argument that small asteroids are preferentially transported to and trapped in the resonance. In Fig. 8, we observe that Massalia, the source of the family, is very close to the 1:2 resonance. Therefore, asteroids could have been injected directly into the resonance by the cratering event that formed Massalia family and some of the asteroids now in the resonance may be the survivors of that event.

We have argued that the Vesta family may have an age comparable with the age of the solar system. Fig. 11c shows that for this family, the change in the mean inclination is zero, but we also observe that there are no significant differences between the asteroids in the libration mask and those outside of the mask: there is no number excess, no change in mean size and no change in mean eccentricity. One difference between this family and the other major families in the IMB, is that Vesta has a comparatively low eccentricity. There are two first-order resonances associated with the 1:2 resonance: one resonance involves the eccentricity of the asteroid, while the other involves the eccentricity of Mars. Our analysis of the distribution of the proper elements of the asteroids in the resonance shows that for $e_{\rm A} \gtrsim 0.1$ the resonances predominantly involve the eccentricity, $e_{\rm A}$ of the asteroid, whereas for $e_{\rm A} \lesssim 0.1$ the resonances predominantly involve the eccentricity, $e_{\rm M}$ of Mars. We conclude that while an analysis of the dynamics of the mean motion resonances in the IMB could yield information on the Yarkovsky timescales, there are important differences between the interactions of the separate family asteroids with these resonances and each family and each resonance needs a separate analysis.

5. Discussion

Our analysis of the distributions of the orbital elements and sizes of the high-inclination non-family asteroids in the inner main belt suggests that these asteroids belong to old ghost families with dispersed orbital elements. The observations that support this conclusion are: (1) the lack of small asteroids; (2) the mean size of the asteroids increases with increasing orbital inclination; and (3) the CC and NC asteroids in the population, as defined by their WISE albedos, have significantly different proper eccentricity and proper inclination distributions. This analysis supports the work of Delbó *et al.* (2019) who, using independent arguments, reached some of the same conclusions. They searched for correlations between the semimajor axes and the inverse sizes of asteroids and found evidence for two previously unknown families in the inner main belt among the moderate-albedo X-complex asteroids. Delbó *et al.* (2017) also detected a small, old family of large dark asteroids in the inner main belt.

We have shown that the action of Yarkovsky forces driving small asteroids to the ν_6 secular resonance and the 3:1 Jovian mean motion resonance can account for the observation that the mean size of these asteroids increases with increasing orbital inclination. However, if we assume that the Yarkovsky forces acted on the asteroids over the age of the solar system, then the Yarkovsky timescale obtained from the observed size-inclination correlation is much longer than that expected from observations of the orbital evolution of NEAs. We conclude that either the spin directions of the asteroids were not constant over the age of the solar system, or that these asteroids originate from the disruption of larger asteroids and their ages are therefore less than the age of the solar system, or that both explanations are valid. However, we note that the CC and NC asteroids in the inner belt, as defined by their WISE albedos, have significantly different proper eccentricity and proper inclination distributions and this suggests that all the asteroids in the inner belt originate from a small number of large asteroids. This result has implications for the number of root sources of meteorites and NEAs.

https://doi.org/10.1017/S174392132100140X Published online by Cambridge University Press

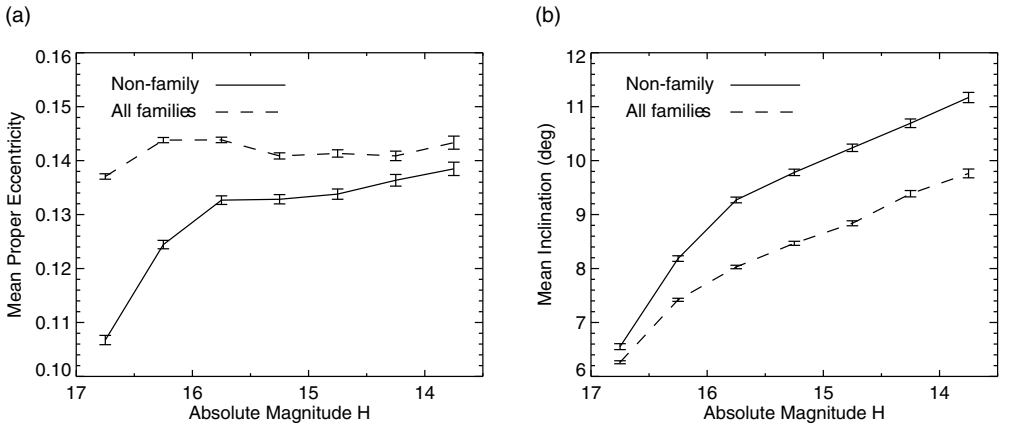

Figure 12. Variation with absolute magnitude, H of the mean proper eccentricity and the mean proper inclination of the family and non-family asteroids in the central main belt with $2.50 < a < 2.82$ au.

For asteroids in the inner belt with absolute magnitudes in the range $13.5 < H < 16.5$, we have shown that Yarkovsky transport of asteroids to the resonant escape hatches is the dominant asteroid loss mechanism and that other, inclination-independent, loss mechanisms have only a small effect on the observed SFD, and no effect on the observed asteroid size-inclination correlation. This result implies that the initial mass of the inner belt was like that of the present inner belt. However, the current observational completeness of the IMB is less than $H = 18$, and until that higher completeness limit is achieved it may be difficult to constrain the collisional and rotational disruption timescales. We have discussed the distribution of asteroids in $a - 1/D$ space and suggested that these distributions could give information on the timescale for changes in the spin directions and on the collisional disruption timescales. We note that the same information could be obtained from an analysis of the distributions of family asteroids in proper orbital element space. For example, Pavela *et al.* (2014) have analysed the evolution of the Karma family asteroids in $a - I$ space and shown that some regions of this space appear to lack small asteroids. They suggested that this could be due to observational incompleteness, but another explanation for this interesting result is that some small asteroids are absent because they have been disrupted. If that is the case, then knowing the age of the family, we should be able to constrain the asteroid loss timescale.

If we allow that the asteroids in the Vesta family, like those in the putative inner belt ghost families, have experienced collisional disruptions and/or changes in their spin directions, then the observed size frequency distribution of the Vesta family can be accounted for by the action of Yarkovsky forces, but only if, in addition, the age of this family is comparable to the age of the solar system. This result conflicts with an estimate of the age of the family that has been derived from surface crater counts, a result obtained by assuming that the population of impactors in the solar system has remained constant. Thus, our result calls into question the reliability of that dating method. To derive the age of the Vesta family, we have assumed that the initial SFD was linear on a log-log scale, an assumption that is supported by the observed SFD of the young Massalia family. From our analysis, we deduce that the initial slope of the Vesta family SFD was similar to that of the Massalia family, but we have not given a reason why families created by cratering events should necessarily have similar initial SFDs.

In this paper, we have only discussed the observed correlations of the orbital elements and asteroid sizes in the IMB, but these correlations are not confined to the IMB. In Fig. 12, we show that for the asteroids in the central main belt, with semimajor axes

https://doi.org/10.1017/S174392132100140X Published online by Cambridge University Press

in the range $2.50 < a < 2.82$ *au*, the mean proper inclination of the non-family asteroids increases with mean asteroid size. We observe that the correlations for the family and non-family asteroids are similar, suggesting that some of the non-family asteroids are halo asteroids, but this needs further analysis. In the central main belt, we do not have a configuration of secular and mean motion resonances like that which exists in the IMB, so it may be that ghost families with different mean proper eccentricities and mean proper inclinations and different SFDs determine the observed correlations.

Acknowledgements

Figures 1, 3, 4, 7 and 8 in this paper are adapted from Dermott *et al.* (2021).

References

Christou, A., Dermott, S., & Li, D. 2020, in: *AAS/Division of Dynamical Astronomy Meeting*, 52, 100.05.
Delbó, M., Walsh, K., Bolin, B., Avdellidou, C., & Morbidelli, A. 2017, *Science*, 357, 1026.
Delbó, M., Avdellidou, C., & Morbidelli, A. 2019, *A&A*, 624, A69.
Dell'Oro, A., Boccenti, J., Spoto, F., Paolicchi, P., & Knežević, Z. 2021, *MNRAS*, 506, 4302.
DeMeo, F.E., & Carry, B. 2014, *Nature*, 505, 629.
Dermott, S.F., Christou, A.A., Li, D., Kehoe, T. J.J., & Robinson, J.M. 2018, *Nature Astronomy*, 2, 549.
Dermott, S.F., Li, D., Christou, A.A., Kehoe, T. J.J., Murray, C.D., & Robinson, J.M. 2021, *MNRAS*, 505, 1917.
Dohnanyi, J.S. 1969, *Journal of Geophysical Research*, 74, 2531.
Durda, D.D., & Dermott, S.F. 1997, *Icarus*, 130, 140.
Eugster, O., Herzog, G.F., Marti, K., & Caffee, M.W. 2006, in: Lauretta, Dante S. & McSween, H.Y. (eds.), *Meteorites and the Early Solar System II*, 829
Farinella, P., Froeschlé, C., Froeschlé, C., Gonczi, R., Hahn, G., Morbidelli, A., & Valsecchi, G.B. 1994, *Nature*, 371, 314.
Farinella, P. & Vokrouhlický, D. 1999, *Science*, 283, 1507.
Farnocchia, D., Chesley, S.R., Chodas, P.W., Micheli, M., Tholen, D.J., Milani, A., Elliott, G.T., & Bernardi, F. 2013, *Icarus*, 224, 192.
Gallardo, T. 2007, *Icarus*, 190, 280.
Gallardo, T., Venturini, J., Roig, F., & Gil-Hutton, R. 2011, *Icarus*, 214, 632.
Gladman, B.J., Migliorini, F., Morbidelli, A., Zappala, V., Michel, P., Cellino, A., Froeschle, C., Levison, H.F., Bailey, M., & Duncan, M. 1997, *Science*, 277, 197.
Granvik, M., Morbidelli, A., Vokrouhlický, D., Bottke, W.F., Nesvorný, D., & Jedicke, R. 2017, *A&A*, 598, A52.
Granvik, M., Morbidelli, A., Jedicke, R., Bolin, B., Bottke, W.F., Beshore, E., Vokrouhlický, D., Nesvorný, D., & Michel, P. 2018, *Icarus*, 312, 181.
Greenberg, A.H., Margot, J.L., Verma, A.K., Taylor, P.A., & Hodge, S.E. 2020, *AJ*, 159, 92.
Hendler, N.P. & Malhotra, R. 2020, *The Planetary Science Journal*, 1, 75.
Jacobson, S.A., Marzari, F., Rossi, A., Scheeres, D.J., & Davis, D.R. 2014, *MNRAS* (Letters), 439, L95.
Jenniskens, P. 2018, in: *AAS/Division of Dynamical Astronomy Meeting*, 49, 102.04.
Jenniskens, P. 2020, in: *IAU General Assembly*, 30, 9.
Jenniskens, P., Gabadirwe, M., Yin, Q-Z., et al. 2021, *Meteoritics & Planetary Science*, 56, 844.
Knežević, Z., & Milani, A. 2000, *Cel. Mech. Dyn. Astr.*, 78, 17
Kruijer, T.S., Burkhardt, C., Budde, G., & Kleine, T. 2017, *PNAS*, 114, 6712.
Marchi, S., McSween, H.Y., O'Brien, D.P., Schenk, P., De Sanctis, M.C., Gaskell, R., Jaumann, R., Mottola, S., Preusker, F., Raymond, C.A., Roatsch, T., & Russell, C.T. 2012, *Science*, 336, 690.
Marzari, F., Rossi, A., Golubov, O., & Scheeres, D.J. 2020, *AJ*, 160, 128.
Masiero, J.R., Grav, T., Mainzer, A.K., Nugent, C.R., Bauer, J.M., Stevenson, R. & Sonnett, S. 2014, *ApJ*, 791, 121.

McSween, H.Y., Mittlefehldt, D.W., Russell, C.T., & Raymond, C.A. 2013, *Meteoritics & Planetary Science*, 48, 2073.
Migliorini, F., Michel, P., Morbidelli, A., Nesvorný, D., & Zappala, V. 1998, *Science*, 281, 2022.
Milani, A., Cellino, A., Knežević, Z., Novaković, B., Spoto, F., & Paolicchi, P. 2014, *Icarus*, 234, 46.
Minton, D.A. & Malhotra, R. 2010, *Icarus*, 207, 744.
Morbidelli, A. & Nesvorný, D. 1999, *Icarus*, 139, 295.
Morbidelli, A., Delbo, M., Granvik, M., Bottke, W.F., Jedicke, R., Bolin, B., Michel, P., & Vokrouhlicky, D. 1997, *Icarus*, 340, 113631.
Murray, C.D. & Dermott, S.F. 1999, *Solar System Dynamics*, Cambridge University Press, Cambridge.
Nesvorný, D. 2015, HCM Asteroid Families V3.0. *NASA Planetary Data System.*
Nesvorný, D., Brož, M., & Carruba, V 2015, in: Michel, P., DeMeo, F.E., & Bottke, W.F. (eds.), *Asteroids IV*, 297.
Nugent, C.R., Margot, J.L., Chesley, S.R., & Vokrouhlický, D. 2012, *AJ*, 144, 60.
Pavela, D., Novaković, B., Carruba, V., & Radović, V, 2021, *MNRAS*, 501, 356.
Spoto, F., Milani, A., & Knežević, Z. 2015, *Icarus*, 257, 275.
Vokrouhlický, D. & Farinella, P. 2000, *Nature*, 407, 606.
Walsh, K.J., Morbidelli, A., Raymond, S.N., O'Brien, D.P., & Mandell, A.M. 2011, *Nature*, 475, 206.
Wisdom, J. 1985, *Nature*, 315, 731.
Zappala, V., Cellino, A., Farinella, P., & Knežević, Z. 1990, *AJ*, 100, 2030.